Impact of Frictional Heat Generation upon Temperature of Sesame Paste Flow through Screw-expeller

R. Shanthini[1], S. A. V. Kumar[2], S. M. D. T. Sandaruwan[1]

[1] Department of Chemical and Process Engineering, University of Peradeniya, Peradeniya, Sri Lanka
[2] Texlan Center (Pvt) Ltd, Dagonna Road, Minuwangoda, Sri Lanka

Abstract:

Temperature of sesame paste flowing through a screw-expeller was studied. Screw-expeller used consisted of a rotating tapered screw and a constant-inner-diameter stationary barrel. Since screw diameter was much larger than the sesame paste thickness, an unwrapped model was employed with Cartesian coordinate x taken parallel to the barrel surface, y taken perpendicular to screw flights and z taken from screw root to barrel. Steady, fully developed, incompressible, creeping flow was assumed. Sesame paste was observed to exhibit shear thinning behaviour characterized by K, the consistency coefficient, and n, the power-law index. Mass, momentum and energy balance equations available in the computational fluid dynamics (CFD) module of COMSOL Multiphysics® were used. In the past literature, no-slip was assumed at the paste/barrel and paste/screw interfaces and viscous heat generation was taken as the major heat source. In this study, slip at the paste/barrel interface and the resulting frictional heat generation at the said interface (Q_F) were considered. Q_F is characterized by λ, the coefficient of friction at the paste/barrel interface, and β, the slip factor at paste/barrel interface. Owing to the reduction in sesame paste thickness along x-direction, choice of mesh was crucial to the accuracy of the temperature field simulated and therefore a user-controlled mesh was used. Extra fine-sized free triangular mesh was created on the barrel surface boarded by extremely fine-sized mesh on either sides and they were swept down to the screw root surface through 20 fixed number of elements so that the reducing thickness of the sesame paste was adequately represented for numerical simulation. Taguchi method was utilised to design the simulation study on the impact of β, K and n upon the maximum temperature of flow. At $\beta = 0$, Q_F was zero and Q_V raised the flow temperature to a maximum of 0.7˚C above the inlet temperature. As β was increased from 0 to 0.3, Q_F increased, almost linearly, to its highest at 13 W. Maximum temperature also increased, almost linearly, to its highest at 65.9˚C. As the temperatures recorded during the laboratory experiments (subjected to a maximum of 57˚C) were below 65.9˚C, investigations were not extended beyond $\beta = 0.3$. Simulation results showed that Q_F was more sensitive to β than to K and n. This study, therefore, clearly demonstrated the importance of including slip at the boundaries and Q_F when modelling flow through screw-expeller.

Keywords: Screw-expeller model, Sesame oil, Friction, Heat generation

1. Introduction

Modelling the material flow in a screw-expeller has been an area of intense research since long. According to Wang [1], mathematical modelling of flow in a screw-expeller commenced with the work of Rowell and Finlayson [2, 3] who was working with flow through screw viscosity pumps. They assumed the flow to be steady, laminar, fully developed, incompressible and Newtonian without slippage at the walls and with negligible gravitational effects. Ignoring the curvature effects, they unwrapped the helical screw channel into a rectangular channel and assumed non-zero flow velocity components in the screw channel direction and the direction perpendicular to the flights. They solved the reduced partial differential equations (Navier-Stokes equations [4]) analytically to determine the two velocity components and pressure. In dealing with plastics extrusion, Mori and Matsumoto [5] were the first to model the non-Newtonian nature of the flow in screw-expellers. Martin [6] was the first to solve the governing equations numerically using a computer. He used a power-law model and

considered all 3 velocity components of the flow, assumed to be fully developed, in an unwrapped straight rectangular channel.

Mrema and McNulty [7] modelled the fundamentals of oil expression by a mathematical model based on Hagen Poiseulle equation, Darcy's law and a modified form of Terzaghi's equation. Gopalakrishna et al [8] numerically simulated the heat and momentum transfers inside the screw channel for a power-law fluid. Finite difference computations were carried out to solve the governing set of partial differential equations for the velocity and temperature fields over a wide range of governing parameters. Omobuwajo et al [9] carried out an experimental study and pointed out the importance of thermal effects on the modelling of the screw press operation.

In this study, analysis of Gopalakrishna et al [8] was followed, with necessary modifications, for mathematical modelling of the temperature of sesame oil expressed in a screw-expeller. In past literature inclusive of [8], in general, no-slip condition was assumed to prevail at all boundaries and viscous heat dissipation was taken as the major heat source to model temperature of the flow. Following Wang [1], slip of the flow at the walls was introduced in this study. Slip at rough surfaces causes friction. Frictional heat generation at the paste/barrel interface was modelled for the first time in this study. Frictional heat was taken as a product of coefficient of friction, pressure at the slipping boundary and slip velocity at the boundary. Focus of Wang [1] had been the relationship between discharge pressure and discharge rate for canola paste flow. In this study, focus was the temperature of sesame seed paste flowing through a single screw extruder. Model developed was simulated using COMSOL Multiphysics®. Taguchi method was utilised to design the experimental study on the impact of degree of slip and power-law constants upon maximum temperature in the flow.

2. Materials and Methods

2.1 Screw expeller used

Screw-expeller used consisted of a rotating screw and a stationary barrel. Photograph of the screw used is shown in Figure 1. Screw sections separated by screw flights were numbered as i = 1 to 11 as shown in Figure 1. Screw root was tapered starting from the left end of screw section 2 to the right end of screw section 11. Screw root diameter at the left end of screw section 2 (denoted by Dsr_1) was 14.50 mm and the corresponding screw flight height (denoted by h_1) was 2.75 mm, which gave a screw flight diameter (denoted by D_s) of 20.00 mm. Screw root diameter at the right end of screw section 11 (denoted by Dsr_{11}) was 18.44 mm and the corresponding screw flight height (denoted by h_{11}) was 0.78 mm, which gave the same screw flight diameter of 20.00 mm. Ratio of flight height to screw diameter varied from h_1/D_s (= 0.14) to h_{11}/D_s (= 0.04), respectively, and, therefore, screw used was assumed to have a screw flight diameter much larger than the screw flight height (i.e., $D_s >> h_i$).

Screw pitch (denoted by P_i) is the axial distance between adjacent screw flights and was 14.50 mm. Distance between the cross sections corresponding to Dsr_1 and Dsr_{11} was then 10 times P_i, which gave 145.0 mm. Axial screw flight width (denoted by e) was 3.20 mm and, therefore, axial screw channel width was given as follows:

$$W_{axial} = P_i - e = 11.30 \text{ mm} \quad (1)$$

Taper angle of the screw (denoted by ϕ) is the angle made by the tapered screw surface with the screw axis and was given as follows:

$$\phi = \tan^{-1}[(Dsr_{11}-Dsr_1)/(2x10xP_i)] = 0.78 \text{ deg} \quad (2)$$

Helix angle (denoted by θ) is the angle screw flight makes with the normal to screw axis and was given as follows:

$$\theta = \tan^{-1}[P_i/(\pi D_s)] = 13.00 \text{ deg} \quad (3)$$

Photograph of screw placed within the barrel is shown in Figure 2. Screw sections 1, 2 and part of 3 could be seen at the screw feed end and the remaining screw sections are covered by the barrel surface. Screw flights in the first four screw sections did not make contact with the inner surface of the barrel. Screw flights in the remaining 7 screw sections were tightly fitted by the barrel inner surface having a diameter (denoted by D_b) of 20.00 mm.

Since screw was tapered, cross-sectional area of screw channel decreased along x-direction. Sesame seeds moving along such channel were subjected to increasing pressure and seeds got

crushed under pressure. Crushed sesame got sheared by rotating screw. Consequently, oil trapped within the seeds got expelled and the expelled oil was free to leave through oil exit slits such as the oil exit slit EF shown in Figure 2 and three similar slits placed at 90, 180 and 270 degrees from slit EF on barrel section consisting of slit EF. Slits cover screw sections 6, 7 and 8.

Remains of sesame (referred to as cake) continued to move through the last three screw sections beyond Point F and cake left at the cake exit end (shown in Figure 2) via the circular outlet bounded by the outer surface of screw root and the inner surface of screw barrel.

2.2 Governing equations

Sesame flowing through the channel was assumed to be a homogeneous mixture of crushed sesame seeds and the expelled oil, which will be referred to as sesame paste. Sesame paste flow along the screw channel from the left end of screw section 2 to the right end of screw section 8 (i.e., up to Point F) was assumed to resemble fluid flow and modelled using mass, momentum and energy transport equations describing fluid flow [4].

Even though it was possible for oil to leave the slits via the entire lengths of the slits, oil was assumed to leave the channel mostly at the right ends of the slits (i.e., at Point F and its three counterparts), which was the end of screw section 8. Following the approach taken by Gopalakrishna et al [8], among others, laminar flow was assumed and continuity equation, momentum balance and energy balance, Equations (4), (5) and (6), respectively, were used to model steady, creeping flow of sesame paste which was assumed to be incompressible and non-Newtonian.

$$\nabla \cdot \bar{U} = 0 \quad (4)$$

$$\nabla p = \nabla \cdot (2\mu \check{D}) \quad (5)$$

$$\rho C_p(\bar{U} \cdot \nabla T) = \nabla \cdot (k \nabla T) + Q_V \quad (6)$$

where the dependent variables to be solved for were velocity vector ($\bar{U}$), pressure (p) and temperature (T) and properties of sesame paste to be specified were apparent viscosity (μ), density (ρ), specific heat (C_p) and thermal conductivity (k). Strain tensor ($\check{D}$) is expressed in terms of velocity gradient by Equation (7) and heat generation owing to the viscous forces acting within the fluid (Q_V) is expressed by Equation (8).

$$\check{D} = \tfrac{1}{2} [\nabla \bar{U} + (\nabla \bar{U})^T] \quad (7)$$

$$Q_V = 2\mu \check{D} : \nabla \bar{U} \quad (8)$$

Sesame paste was observed to exhibit shear thinning behaviour [10, 11] described by Equations (9).

$$\mu = K [(\check{D}: \check{D})^{1/2}]^{n-1} \quad (9)$$

where K is consistency coefficient, n is power-law index and $[(\check{D}: \check{D})^{1/2}]$ is shear rate.

2.3 Unwrapped channel assumption

Since the screw diameter was much larger than the sesame paste thickness, an unwrapped model was employed ([1], [8], [12] and [13] among others). Figure 3 shows the schematic diagram of the unwrapped model (not drawn to scale). Cartesian coordinate system was used with coordinate x taken parallel to the barrel surface. Velocity components of $\bar{U}$ along x, y and z directions were taken as u, v and w, respectively. Screw channel width perpendicular to the flights was given as follows:

$$W = W_{axial} \cos\theta = 11.01 \text{ mm} \quad (10)$$

The unwrapped length of screw channel per each screw section (denoted by L_s) was given as follows:

$$L_s = \pi D_s / \cos\theta = 64.48 \text{ mm} \quad (11)$$

Height of screw channel at the inlet of the unwrapped channel corresponded to the height of screw flight to the left of the second screw section and, therefore, it was given by h_1 (= 2.75 mm). Height of screw channel along x-direction was a variable given as follows:

$$h = h_1 - x \tan\varphi \quad (12)$$

where φ is the taper angle of the unwrapped screw channel and was given as follows:

$$\varphi = \tan^{-1}[(h_1 - h_{11})/(10\, L_s)] = 0.18 \text{ deg} \quad (13)$$

Total length of the screw channel considered (denoted by L_T) consisted of screw sections 2, 3, 4, 5, 6, 7 and 8 and, therefore, was given as follows:

$$L_T = (8\text{-}1)\, L_s = 451.36 \text{ mm} \quad (14)$$

Height of screw channel at the outlet of the unwrapped channel corresponded to the height of screw flight to the right of the eighth screw section and, therefore, was given as follows:

$$h_8 = h_1 - L_T \tan\varphi = 1.37 \text{ mm} \quad (15)$$

2.4 Boundary conditions

In the past literature ([8] and [12] among others), barrel was assumed to rotate in relation to screw which was assumed to be stationary and no-slip was assumed at all paste/solid interfaces. Flow boundary conditions used were, therefore, as follows:

At the screw root and flight surfaces:

$$u = v = w = 0 \quad (16)$$

At the barrel surface:

$$u = (\pi D_b N/60) \cos\theta \quad (17a)$$

$$v = -(\pi D_b N/60) \sin\theta \quad (17b)$$

$$w = 0 \quad (17c)$$

where N was the screw rotational speed in revolutions per minute (rpm) and ($\pi D_b N/60$) was the velocity of "rotating barrel" relative to "stationary screw". Wang [1] reasoned out occurrence of material slip at the barrel surface and modified the boundary condition at the barrel as follows:

$$u = (1-\beta)(\pi D_b N/60) \cos\theta \quad (18a)$$

$$v = -(1-\beta)(\pi D_b N/60) \sin\theta \quad (18b)$$

$$w = 0 \quad (18c)$$

where β is the slip factor and $\beta = 0$ for no-slip conditions and $\beta = 1$ for total slip. Equations (16) and (18) were adopted as flow boundary conditions.

In the past literature ([8], [13] and [14] among others), adiabatic condition was assumed at the screw root and flights boundaries and isothermal conditions or heat influx by heating the barrel were assumed at the barrel boundary. Since screw was made up of stainless steel, adiabatic boundary conditions at the screw root and flights boundaries were retained. As for the barrel boundary condition, frictional heat generation at the paste/barrel interface across screw sections 5, 6, 7 and 8 was considered. It was because inner barrel surface across the said screw sections was observed to be rough. Frictional heat generation at the paste/barrel interface was quantified, adopting the suggestion made by Kennedy [15] for a general situation, as follows:

$$Q_F = \int\int (\lambda\, p_{barrel}\, \beta\, \pi\, D_b N/60)\, dy\, dx \quad (19)$$

where λ is coefficient of friction at the slipping interface, p_{barrel} is the pressure acting at the barrel boundary and limits of integrations are L_p to L_T in x-direction and 0 to W in y-direction. L_p (= $3L_s$) was the length of the unwrapped channel corresponding to the screw sections 2, 3 and 4. Normal stress acting on the barrel boundary, given by $\mu(\partial w/\partial z)_{barrel}$, was found to be negligibly small and was, therefore, not included in Equation (19).

At $\beta = 0$, sesame paste velocity is the same as "barrel velocity" and, hence, no slip at the paste/barrel interface and $Q_F = 0$. At $\beta \neq 0$, sesame paste slips at paste/barrel interface and, therefore, Q_F was non-zero. All heat generated was assumed to enter the sesame paste by imposing adiabatic boundary condition at the paste/barrel interface. To the best of authors' knowledge, frictional heat generation was used as a boundary condition of flow through screw-barrel in just one other journal paper [16] in which frictional heat was not modelled but experimentally estimated values were used. At the inlet, ambient pressure and ambient temperature were assumed.

2.5 Simulation

Model developed was fed to COMSOL simulation package. Extra fine-sized free triangular mesh was created on the barrel surface boarded by extremely fine-sized mesh on either sides and they were swept down to the screw root surface through 20 fixed number of elements so that the narrowing height of the sesame paste was adequately represented for numerical simulation. The choice of mess was guided by sensitivity analysis. Complete mesh consisted of 336880 domain elements, 98168 boundary elements, and 6688 edge elements.

Simulation results were considered meaningful only if the following two conditions were satisfied:

Condition 1: Seeds fed at ambient pressure to the screw expeller should get pressurized as they moved along the screw channel. It was, therefore, pressure must increase along x-direction or at least along part of x-direction.

Condition 2: Mass flow rates of sesame paste at the inlet (m_{in}) and at the outlet (m_{out}) should take positive values and equal each other, where m_{in} and m_{out} are given as follows:

$$m_{in} = \int_0^{h1}\int_0^{W} u\, dy\, dz$$

$$m_{out} = \int_0^{h8}\int_0^{W} u\, dy\, dz$$

2.6 Parameters used

Densities of oil and solids in sesame paste made from milled, roasted, hulled sesame seeds were 900 and 1390 kg/m^3, respectively [10]. Densities of oil and solids in sesame paste made from milled, hulled sesame seeds roasted at 150˚C for 100 min were 944 and 1321 kg/m^3, respectively [11]. Roasting and dehulling could have reduced density of solids in sesame paste. As unhulled, unroasted sesame seeds were used, a sesame paste density of 1400 kg/m^3 was chosen to represent sesame paste.

In the temperature range of 25 to 70˚C and the moisture content range of 3 to 20% dry basis, specific heat ranged from 900 to 3060 J/kg.^{o}C and thermal conductivity ranged from 0.023 to 0.149 W/m.˚C for white and brown sesame seed varieties [17[. Averaged C_p and k values of 1996 J/kg.˚C and 0.0845 W/m.˚C, respectively, to represent sesame paste since the composition of sesame paste would be the same as that of the seeds until oil was separated from the sesame paste.

Following the procedure laid out in Darvishi [18], λ of sesame paste was determined in triplicate at six different sections of the screw used. Mean λ was estimated at 0.66±0.12.

For sesame paste made from roasted hulled sesame seeds, K varied in the range of 1 to 2.5 Pa.s^n and n varied in the range of 0.82 to 0.88 in the temperature range of 30 to 70˚C and shear rates range of 0.13–500 s^{-1} [10]. For sesame pastes made from unhulled sesame seeds roasted at 130˚C for 210 min, K varied in the range of 9.36 to 28.08 Pa.s^n and n varied in the range of 0.47 to 0.53 in the temperature range of 15 to 65˚C [19].

One and only reference available on β for seed paste processed in a screw expeller was about canola paste [1] and β values determined were 0.041, 0.046, 0.085 and 0.26 for canola paste concentrations of 35.3, 64.5, 95.7 and 146 g solid per 100 g liquid, respectively.

Owing to the wide ranges of K (1 to 28 Pa.s^n) and n (0.5 to 0.9) reported in the literature and the lack of K and n data for sesame paste from unroasted seeds with hull and since β for sesame paste was not known, a Taguchi design of experiment was carried out to determine the impact of different K, n and β upon the paste flow characteristics.

Screw rotational speed used was 50 rpm. Ambient pressure was taken as 1 bar and ambient temperature as 27˚C.

2.7 Experimental data acquisition

Experiments were carried out with sesame seeds of 3.6, 4.6, 5.1, 6.3 and 7.0% dry basis moisture contents as described in detail in the postgraduate diploma thesis of Abeysekara [20]. Seeds used were with hull and were not roasted. Oil samples were extracted in triplicate using the screw-expeller operated at 50 rpm. Mass flow rate and temperature of oil leaving the oil exit were recorded. These two data were used for verifying the numerical model developed.

3. Results and Discussion

3.1 Experimental results

From the experimental measurements made [20], mass flow of sesame seeds fed to the screw-expeller at the seed feed end (Figure 2) and average temperature of oil leaving the oil slit at Point F (Figure 2) were obtained. Mean mass flow rate of seeds was 2.27±0.06 kg/h with 3% coefficient of variation. Mean temperature of oil at its exit was 57±3˚C with 5% coefficient of variation. Coefficient of variations as low as 3 and 5% revealed that seed moisture content had negligibly small influence upon mass flow rates and temperature of oil leaving screw-expeller. Simulation results were verified against the above-stated means.

3.2 Impact of exit pressure

Simulations were carried out to study the impact of varying exit pressure (denoted by p_{exit}) upon fluid flow characteristics under the assumptions of no slip at the barrel (β = 0) and Newtonian behaviour of sesame paste (n = 1). For n = 1, K became μ. Responses estimated were the maximum values of T and p in the entire flow domain and mass flow rate of sesame paste at the inlet and outlet. Results obtained at μ = 100 and 1000 Pa.s were tabulated in Table 1 and they satisfied the two conditions laid down in Section 2.5: pressure increased from 1 bar at the inlet to maximum pressures above 8.1 bar in all cases analysed;

mass flow rates in and out were the same at two decimal place accuracy.

Table 1 shows that, for μ = 1000 Pa.s, maximum temperatures were 19˚C above the inlet temperature of 27˚C for all cases of p_{exit} studied. That was a 70% increase in temperature. Energy required to raise the temperature could have come from 3 sources. One was Q_F at the paste/barrel interface. Since β = 0, there was no slip at the paste/barrel interface and, therefore, Q_F = 0. Second was the energy flow from the surroundings which was zero since adiabatic conditions were assumed at the boundary walls. Hence, energy required to raise the temperature had come from the third source which was Q_V within the fluid which was substantial in case of μ being as high as 1000 Pa.s. Table 1 also shows that, for μ = 100 Pa.s, maximum temperatures tabulated were only 1 to 2˚C above the inlet temperature of 27˚C for all cases of p_{exit} studied. It meant viscous heat generation was negligibly small even when the flow viscosity was as high as 100 Pa.s. In case of sesame paste, such high viscosities were not reported in the literature (Section 2.6). It was, therefore, it could be concluded that viscous heat generation was not the cause of temperature increase in sesame being processed in a screw expeller.

3.3 Impact of K, n and β

In order to study the impact of varying K, n and β upon flow characteristics, a 4-factor and 3-level experiment was designed. Factors chosen were p_{exit}, β, K and n. Levels of p_{exit} chosen were 1.5, 3.0 and 5.0 bar. Levels of β were taken at 0.0, 0.15 and 0.30. Levels of K chosen were 10, 50 and 100 Pa.s^n. Levels of n chosen were 0.8, 0.9 and 1.0. There were 81 combinations to be tested if full factorial design was chosen. It was, therefore, the orthogonal array of Taguchi method [21] was adopted which required 9 combinations of the factors considered and the combinations and the corresponding results are tabulated in Table 2. Trends set by varying factors were depicted in the main effects plots of data means given in Figures 4 to 8.

Figure 4 showed that frictional heat generation was more sensitive to β than it was to p_{exit}, K and n. Lowest value of mean of frictional heat generation was zero and it was, of course, for the case of no-slip conditions at the paste/barrel interface (β = 0). As β was increased from 0 to 0.3, mean of frictional heat generation increased, almost linearly, to its highest at 13 W. Frictional heat was the only source of energy available to increase the temperature (as discussed in Section 3.2) and, hence, maximum temperature followed similar pattern.

Figure 5 showed that maximum temperature was more sensitive to β than it was to p_{exit}, K and n. Lowest value of mean of maximum temperature attained was 27.7˚C and it was for the case of no-slip conditions at the paste/barrel interface (β = 0). As β was increased from 0 to 0.3, mean of maximum temperature increased, almost linearly, to its highest at 65.9˚C. As the oil temperatures recorded during the laboratory experiments were below 65.9˚C (Section 3.1), investigations were not extended beyond β = 0.3.

Figure 6 showed that maximum pressure was less sensitive to β than it was to p_{exit}, K and n and it increased, almost linearly, with increasing p_{exit}, K and n. Viscosity of the flow was high at high values of K and n and highly viscous flow could hold its direction against adverse pressure gradients.

Figure 7 showed that mass flow rate was highly sensitive to p_{exit}, β and K and least sensitive to n. Mass flow rate decreased with increasing exit pressure since the pressure gradient was against flow direction. When β = 0, no-slip condition prevailed and, hence, sesame moved with the "rotating barrel" which led to high mass flow rate. As β increased sesame slipped backwards and, hence, mass flow rate was reduced. Viscosity of the flow was high at high values of K and highly viscous flow could hold its direction against adverse pressure gradients. Therefore, mass flow rate was high at high K values.

4. Conclusions

Sesame mass moving through the screw channel was assumed to be a homogeneous mixture of crushed seeds, extracted oil and cake (referred to as sesame paste). Screw

channel, bounded by screw outer surface, barrel inner surface and adjacent screw flights, was assumed to be unwrapped. Sesame paste flow was assumed to be steady, incompressible, creeping flow of non-Newtonian fluid. Continuity equation, momentum balance and energy balance equations were utilized to obtain the governing equations. Barrel was assumed to rotate in relation to screw which was assumed to be stationary. No-slip and adiabatic conditions were assumed at all paste/screw interfaces. Slip was assumed at the paste/barrel interface. Since barrel surface was rough, slip caused frictional heat generation at the said interface. Frictional heat generation was modelled and it was the first time such approach was taken with flow through screw expeller. When working with highly viscous flow such as polymer flow, viscous heat would be of considerable quantity and the modellers found it adequate to explain the temperature rise within the material flow. Viscous heat was totally inadequate to explain any temperature rise in the sesame paste flow since its viscosity was not as high as that of polymer flow. Simulations of the model developed successfully predicted temperature rise in the flow. However, further modifications of the model developed in the study are required to satisfactorily model the mass flow rate through the expeller.

Acknowledgement

National Science Foundation (Sri Lanka) research grant RG/2015/EA&ICT/01 was appreciatively acknowledged.

References

1. Wang F. 1993. Study of single-screw extruders for continuous feeding of canola paste for supercritical fluid extraction. PhD thesis. Canada: The University of British Columbia.
2. Rowell H.S., Finlayson D. 1922. Screw viscosity pumps. Engineering 114: 606–606
3. Rowell H.S., Finlayson D. 1928. Screw viscosity pumps. Engineering 126: 249–385
4. Bird R.B., Stewart W.E., Lightfoot E.N. 1960. Transport Phenomena. John Wiley & Sons.
5. Mori Y., Matsumoto T.K. 1958. Analytical study of plastics extrusion. Rheologica Acta 1:240–242
6. Martin B. 1969. Numerical studies of steady-state extrusion process. PhD thesis. United Kingdom: University of Cambridge
7. Mrema G.C., McNulty P.B. 1985. Mathematical model of mechanical oil expression from oilseeds. Journal of Agricultural Engineering Research 31:361–370
8. Gopalakrishna S., Jaluria Y., Karwe M.V. 1992. Heat and mass transfer in a single screw extruder for non-Newtonian materials. International Journal of Heat and Mass Transfer 35:221–237
9. Omobuwajo T.O., Ige M.T., Ajayi O.A. 1997. Heat transfer between the pressing chamber and the oil and oilcake streams during screw expeller processing of palm kernel seeds. Journal of Food Engineering 31:1–7
10. Altay F.L., Ak M.M. 2005. Effects of temperature, shear rate and constituents on rheological properties of tahin (sesame paste). Journal of the Science of Food and Agriculture 85:105–111
11. Çiftçi D., Kahyaoglu T., Kapucu S., Kaya S. 2008. Colloidal stability and rheological properties of sesame paste. Journal of Food Engineering 87:428–43
12. Chiruvella R.V., Jaluria Y., Karwe M.V. 1996. Numerical simulation of the extrusion process for food materials in a single-screw extruder. Journal of Food Engineering 30:449–467
13. Trufanova N.M., Shcherbinin A.G. 2014. Problem background and mathematical model of polymer movement and melting. World Applied Sciences Journal 29:441–452
14. Kargar A. 2015. Numerical analysis of non-Newtonian fluid flow in single screw extruder and its application in food industry. International Journal of Mining, Metallurgy & Mechanical Engineering 3:93–96
15. Kennedy F.E. 2001. Frictional heating and contact temperatures. In: B. Bhushan (ed.),

Modern Tribology Handbook, Vol 1, pp. 235–272. Boca Raton: CRC Press LLC

16. Mikulandrić R., Vermeulen B., Nicolai B., Saeys W. 2016. Modelling of thermal processes during extrusion based densification of agricultural biomass residues. Applied Energy 184:1316–1331
17. Ashtiani S.-H.M., Emadi B., Sanaei-Moghadam A., Aghkhani M.-H. 2014. Effect of moisture content and temperature on thermal behaviour of sesame seed. The Annals of the University of Dunarea de Jos of Galati 38:87–103
18. Darvishi H. 2012. Moisture-dependent physical and mechanical properties of white sesame seed. American-Eurasian Journal of Agricultural & Environmental Sciences, 12:198–203
19. Akbulut M., Coklar H. 2008. Physicochemical and rheological properties of sesame pastes (Tahin) processed from hulled and unhulled roasted sesame seeds and their blends at various levels. Journal of Food Process Engineering 31:488–502
20. Abeysekara O.C. 2018. Yield, antioxidant quality and oxidative stability of sesame oil produced from sesame seeds of varying water content. Sri Lanka, University of Peradeniya: Postgraduate Diploma in Chemical and Process Engineering Thesis.
21. Montgomery D.C. 2008. Design and analysis of experiments, 7th Edition. John Wiley & Sons.

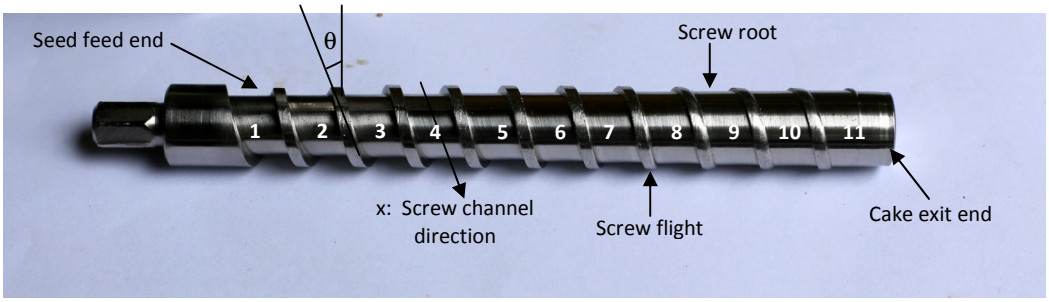

Figure 1 - Photograph of the screw used in the screw expeller. Seed feed end, cake exit end, screw root, screw flight, helix angle (θ) and the screw channel direction (x) are labelled. Screw sections separated by screw flights are numbered from 1 to 11.

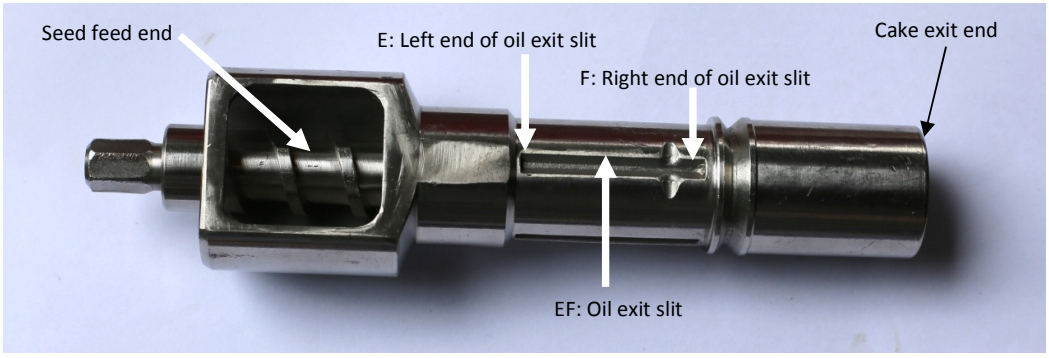

Figure 2 - Photograph of the screw placed within the barrel of the domestic-scale screw expeller (DSE). Seed feed end, cake exit end and the oil exit slit are shown.

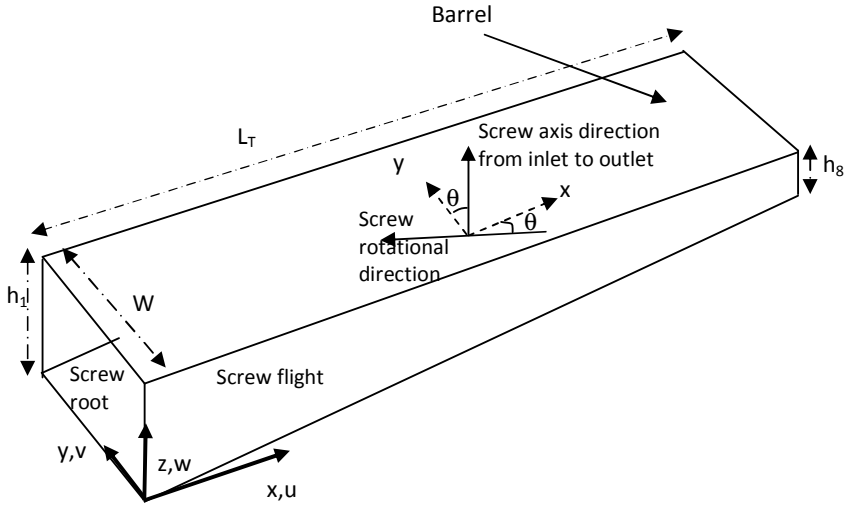

Figure 3 - Schematic diagram of the unwrapped model (not drawn to scale).

Table 1 - Impact of exit pressure (p_{exit}) and apparent viscosity (μ) upon maximum values of temperature (T) and pressure (p) in the entire flow domain, mass flow in (m_{in}) and mass flow out (m_{out}). Slip factor (β) was zero and power-law index n was unity. Pressure and temperature at the inlet were 1.0 bar and 27˚C, respectively.

Control variable		Responses			
		Volume maximum			
μ (Pa.s)	p_{exit} (bar)	T (^oC)	p (bar)	m_{in} (kg/h)	m_{out} (kg/h)
100	1.2	28.8	8.08	2.011	2.011
	2	28.8	8.42	1.984	1.984
	5	28.8	9.86	1.883	1.882
	10	28.9	12.76	1.713	1.713
	20	29.4	21.33	1.378	1.376
1000	1.2	46.0	71.05	2.017	2.017
	2	46.0	71.39	2.014	2.014
	5	46.0	72.64	2.004	2.004
	10	46.0	74.81	1.987	1.987
	20	46.0	79.31	1.954	1.953

Table 2 - Impact of exit pressure (p_{exit}), slip factor (β), consistency coefficient (K) and power-law index (n) upon maximum values of temperature (T) and pressure (p) in the entire flow domain, frictional heat generated at the paste/barrel interface (Q_F) and mass flow out (m_{out}). Pressure and temperature at the inlet were 1.0 bar and 27˚C, respectively.

Factors			Responses			
			Volume maximum			
β	K (Pa.s^n)	n	T (^{o}C)	p (bar)	Q_F (W)	m_{out} (kg/h)
p_{exit} = 1.5 bar						
0.00	10	0.8	27.1	1.58	0.00	1.61
0.15	50	0.9	35.2	3.17	4.85	1.66
0.30	100	1.0	60.4	6.11	17.4	1.40
p_{exit} = 3.0 bar						
0.00	50	1.0	27.9	5.43	0.00	1.88
0.15	100	0.8	39.8	4.51	3.68	1.55
0.30	10	0.9	67.3	3.06	7.97	0.42
p_{exit} = 5.0 bar						
0.00	100	0.9	28.2	7.49	0.00	1.81
0.15	10	1.0	60.9	5.11	5.97	0.36
0.30	50	0.8	69.9	5.19	13.70	0.82

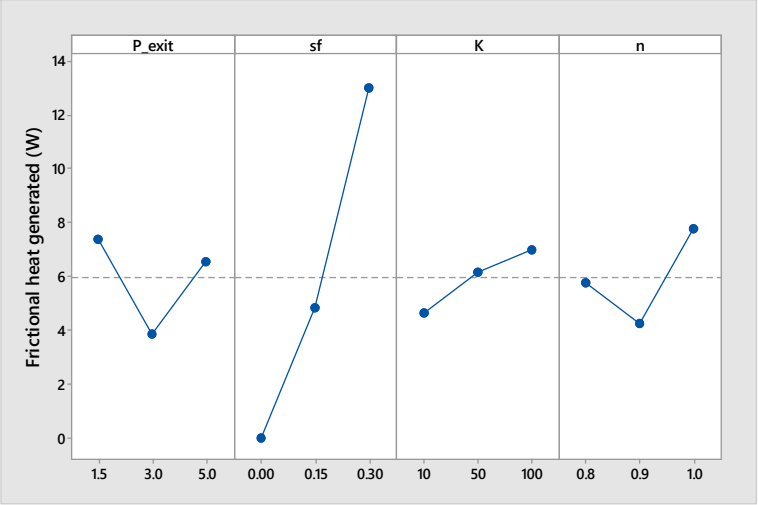

Figure 4 - Data means of frictional heat generated at levels of factors: exit pressure (p_{exit}, in bar), slip factor (sf), consistency coefficient (K, in Pa.s^n) and power-law index (n).

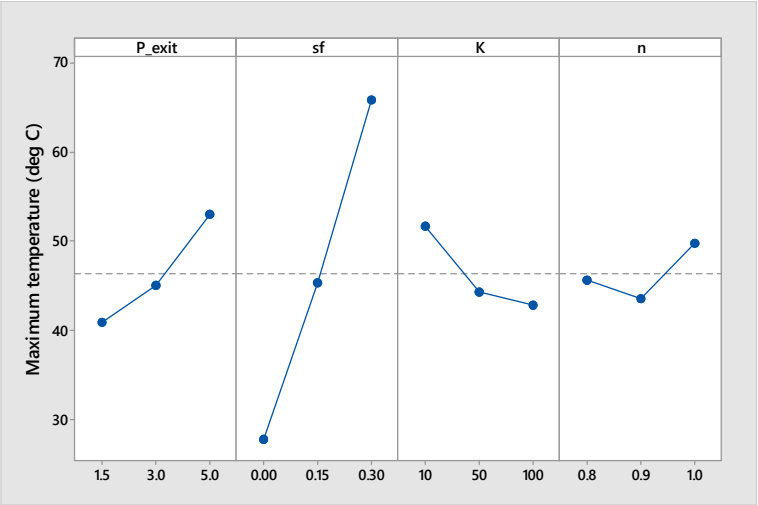

Figure 5 - Data means of maximum temperature at levels of factors: exit pressure (p_{exit}, in bar), slip factor (sf), consistency coefficient (K, in Pa.s^n) and power-law index (n).

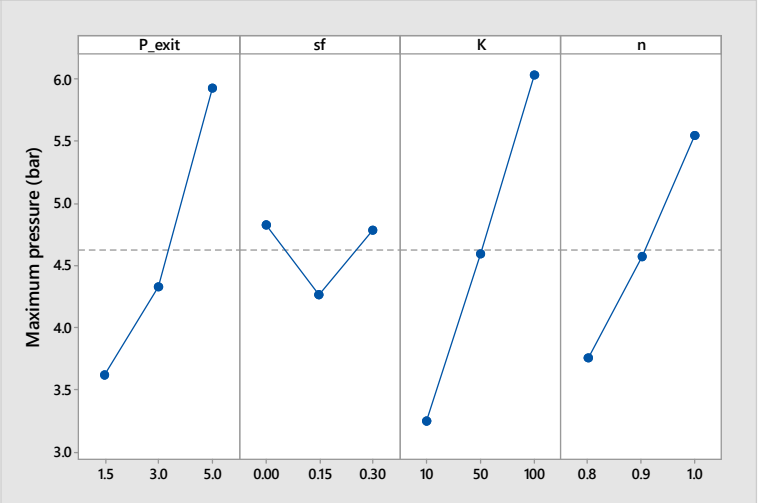

Figure 6 - Data means of maximum pressure at levels of factors: exit pressure (p_{exit}, in bar), slip factor (sf), consistency coefficient (K, in Pa.s^n) and power-law index (n).

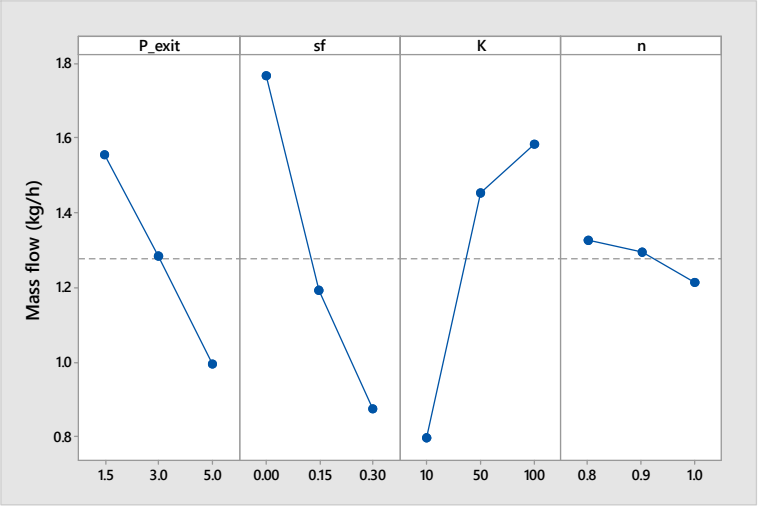

Figure 7 - Data means of mass flow rate at levels of factors: exit pressure (p_{exit}, in bar), slip factor (sf), consistency coefficient (K) and power-law index (n).